The Astrophysical Journal, 599:1196–1206, 2003 December 20
Copyright is not claimed for this article. Printed in U.S.A.

THE FORMATION OF MASSIVE STARS BY ACCRETION THROUGH TRAPPED HYPERCOMPACT H II REGIONS

Eric Keto
Harvard-Smithsonian Center for Astrophysics, 60 Garden Street, Cambridge MA 02138
Received 2003 July 2; accepted 2003 August 28

ABSTRACT

The formation of massive stars may take place at relatively low accretion rates over a long period of time if the accretion can continue past the onset of core hydrogen ignition. The accretion may continue despite the formation of an ionized H II region around the star if the H II region is small enough that the gravitational attraction of the star dominates the thermal pressure of the H II region. The accretion may continue despite radiation pressure acting against dust grains in the molecular gas if the momentum of the accretion flow is sufficient to push the dust grains through a narrow zone of high dust opacity at the ionization boundary and into the H II region where the dust is sublimated. This model of massive star formation by continuing accretion predicts a new class of gravitationally trapped, long-lived, hypercompact H II regions. The observational characteristics of the trapped hypercompact H II regions can be predicted for comparison with observations.

Subject headings: accretion, accretion disks — H II regions — stars: formation

1. INTRODUCTION

The radiation of massive stars profoundly alters their immediate environment by ionizing the surrounding interstellar gas and exerting direct pressure on dust grains in the gas. In the formation of a massive star, there is only a short time, on the order of 10^4 yr, before a contracting massive protostar begins core hydrogen burning and the stellar radiation becomes significant. Thus, for accretion rates less than $10^{-2}\ M_\odot\ \mathrm{yr}^{-1}$, the outward forces of the thermal pressure of the ionized gas and the radiation pressure on dust grains will be competitive with the gravitational attraction of the star during the accretion phase. If the effects of thermal and radiation pressure are capable of reversing the accretion flow within 10^4 yr, then the formation of massive stars by accretion appears problematic.

Following previously suggested hypotheses as to how accretion may proceed despite the effects of significant radiation, this paper explores the possibility and consequences of the formation of massive stars by accretion. In the context of simple models with spherical geometry, the possibility of accretion through the thermal pressure of H II regions was discussed in Walmsley (1995) and Keto (2002a, 2002b, hereafter K02a and K02b, respectively), and the possibilities of accretion through radiation pressure were discussed in Kahn (1974), Yorke (1984, 2001), and Wolfire & Cassinelli (1987). The effects of massive accretion flows onto the protostars themselves have been studied in a series of papers by Beech & Mitalas (1994), Bernasconi & Maeder (1996), Meynet & Maeder (2000), Norberg & Maeder (2000), and Behrend & Maeder (2001). In this paper, the relationships between these hypotheses are explored in the search for a consistent model for massive star formation.

This paper also examines some possibilities for observational confirmation of massive star formation by accretion. In particular, the hypothesis of continuing accretion through trapped H II regions predicts a new class of stable, long-lived, hypercompact (HC) H II regions with specific observable properties. Some approximations allow an easy and accurate calculation of their expected free-free radio continuum flux.

2. THE TRAPPED HYPERCOMPACT H II REGIONS

2.1. *Introduction*

A recent theoretical study of the evolution of H II regions around newly formed stars (K02b) has found that if the stellar gravitational potential is included in the equations that describe the classical model for the pressure-driven expansion of H II regions (Spitzer 1978; Dyson & Williams 1980; Shu 1992), the gravitational force is dominant over the thermal pressure at small scales. These calculations show that a newly formed H II region cannot expand hydrodynamically if its size is smaller than a critical radius ($r < GM/2c^2$) approximately where the escape velocity from the star equals the sound speed, c, of the ionized gas. The H II region is then trapped by the gravitational field of the star. Because the gravitational force is larger than the pressure force, the molecular accretion flow responsible for the formation of the star is not significantly impeded by the thermal pressure of the trapped H II region. Rather, the molecular flow becomes ionized on passing through the ionization front and continues on toward the star. As a result of the continuing accretion, the star will either increase in mass and temperature or more stars will form until the flux of ionizing photons is high enough that the equilibrium boundary of ionization is beyond the critical radius for hydrodynamic expansion. At this point, the H II region begins a rapid transition to the evolution described by the classical model of pressure-driven expansion. The beginning of the expansion essentially ends the accretion flow through the H II region.

2.2. *Size and Timescales of the Trapped* H II *Regions*

Approximate size and timescales can be derived for the long-lived HC H II regions using as a first approximation a simple model for steady-state spherical accretion. In this

TABLE 1
PARAMETERS FOR TRAPPED H II REGIONS

Spectral Type	Mass[a] ($M_\odot$)	UV Flux[a] ($\log s^{-1}$)	Maximum Radius[b] (AU)	Accretion Time[c] (Myr)	Accretion Rate (10^{-4} $M_\odot$ yr^{-1})
B0.5	18.4	47.90	49.5	0.0	0.47
B0	19.5	48.16	52.5	0.02	0.53
09.5	20.8	48.38	56.0	0.05	0.60
09	22.1	48.56	59.4	0.06	0.68
O8.5	23.6	48.72	63.5	0.09	0.77
O8	25.1	48.87	67.5	0.10	0.88
O7.5	26.9	49.00	72.4	0.12	1.01
O7	28.8	49.12	77.5	0.14	1.15
O6.5	30.8	49.23	82.9	0.16	1.32
O6	33.1	49.34	89.0	0.17	1.52
O5.5	35.5	49.43	95.5	0.19	1.75
O5	38.1	49.53	102.5	0.20	2.01

[a] Vacca et al. 1996.
[b] Assumes a temperature of $T = 10^4$ K for the ionized gas and 25 K for the molecular gas.
[c] The accretion times assume a number density at infinity of 1000 cm^{-3} (eq. [2]).

model, a star of mass M with a flux of ionizing photons N_i is at the center of a spherically symmetric, steady accretion flow driven by the gravitational attraction of the star. The self-gravity of the gas is ignored. The stellar radiation maintains an ionized H II region around the star in equilibrium with the recombination rate within the H II region and the mass flux of neutral gas through the H II region boundary. Both the neutral and ionized zones are assumed to be at constant, albeit different, temperatures, and the equation of state in both zones is assumed to be isothermal, with sound speeds c_1 and c_2. With these assumptions, the accretion flow is described by the Bernouilli equation (Bondi 1952; or eq. [2] of K02b).

The maximum size of a trapped H II region is set by the critical radius, where the relative velocity of the static ionization front and the inwardly accelerating molecular accretion flow is equal to approximately twice the sound speed of the ionized gas, $2c_2$. This critical point always occurs just inside the sonic point, $r_c = GM/2c_2^2$, of the ionized flow; therefore, one can say approximately that the H II region is unable to expand unless the sound speed of the ionized gas exceeds the escape velocity from the star. The sonic point is then a first estimate of the maximum size of a trapped H II region for a star of a given mass (Table 1). If there is more than one star in the H II region, for example, a binary, the maximum size of the H II region will scale proportionally with the total mass enclosed within the H II region.

Since a trapped H II region is unable to expand hydrodynamically, it will grow only as the flux of ionizing photons from the star or stars at its center increases and the equilibrium radius of ionization is found at increasingly larger distances. The evolutionary timescale for the H II region in the trapped phase is then set by the rate at which the stars gain mass. In the spherically symmetric model, the accretion rate is

$$\dot{M} = 4\pi\lambda(GM)^2 c_1^{-3}\rho_\infty, \tag{1}$$

where $\lambda = 1.12$, c_1 is the sound speed in the molecular gas, and ρ_∞ is the mass density of the gas at infinity. Although the solution for the accretion flow is found assuming a steady state, if the star gains mass, the accretion rate will change over time. However, as long as the mass does not change more quickly than the accretion flow can adjust, the steady-state approximation will be satisfactory. The time, t, for the star to grow from an initial mass, M_i, to a final mass, M_f, is

$$t = \frac{c_1^3}{4\pi\lambda G^2\rho_\infty}\left(\frac{1}{M_i} - \frac{1}{M_f}\right), \tag{2}$$

or

$$t(\mathrm{Myr}) = 5.8 \times 10^4 \frac{1}{n_\infty(\mathrm{cm}^{-3})}\left[\frac{1}{M_i(M_\odot)} - \frac{1}{M_f(M_\odot)}\right].$$

This simple analysis indicates that the maximum size scales of the trapped H II regions are on the order of 100 AU for single stars or a few hundred AU for binaries and multiplets, and the minimum evolutionary timescales are 10^5–10^6 yr.

2.3. *Evolution of the trapped* H II *regions*

In § 2.2, the size and timescales for the trapped H II regions assumed that the H II region was at the maximum size allowed in the trapped phase. The actual size of a trapped H II region will depend on the mass of the star, its ionizing flux, and the density of the molecular gas. The location of the ionization front is determined by the equation of ionization equilibrium, which must be solved self-consistently with the density and velocity profiles of the ionized accretion flow set by the energy equation governing the flow (§ 3.1 of K02b). The equation of ionization equilibrium yields three possible outcomes for any given set of model parameters. First, if the ionizing flux is weak relative to the accretion rate ($N_i m_{\mathrm{H}}/\dot{M} < 1$), then there will be no H II region. This situation corresponds to a "quenched" H II region. Second, if the ionizing flux and the recombination rate balance at some radius less than the critical radius, the result is a trapped H II region. Or last, if the ionizing flux is strong enough that the radius of ionization equilibrium is beyond the critical point, then the H II region will be rapidly expanding by thermal pressure. As a massive star at the center of an accretion flow continues to gain mass, the ionization equilibrium may pass through all the outcomes above,

TABLE 2
EVOLUTION OF H II REGIONS AROUND SINGLE STARS

Spectral Type	$n_\infty = 150\ \mathrm{cm}^{-3}$ (AU)	$n_\infty = 200\ \mathrm{cm}^{-3}$ (AU)	$n_\infty = 250\ \mathrm{cm}^{-3}$ (AU)
B0.5	1	Q	Q
B0	3	Q	Q
09.5	10	1	Q
09	26	3	1
O8.5	46	5	1
O8	94	10	2
O7.5	E	15	2
O7	E	21	3
O6.5	E	27	4
O6	E	32	4
O5.5	E	33	4
O5	E	36	5

NOTES.—Evolution of an H II region around a single star that is accreting mass and growing in spectral type. The numbers in the table indicate the radius of the trapped H II region around the star. The letter Q indicates that the H II region is quenched, meaning that there is no solution for ionization equilibrium because the ionizing flux is too small compared to the accretion rate. The letter E means that the H II region is no longer trapped but expanding. The growth of the star stops once the H II region begins expanding.

TABLE 4
EVOLUTION OF H II REGIONS AROUND EQUAL-MASS BINARY STARS

Spectral Type	$n_\infty = 50\ \mathrm{cm}^{-3}$ (AU)	$n_\infty = 75\ \mathrm{cm}^{-3}$ (AU)	$n_\infty = 100\ \mathrm{cm}^{-3}$ (AU)
B0.5	16	1	Q
B0	83	3	Q
09.5	E	11	1
09	E	37	3
O8.5	E	72	5
O8	E	115	11
O7.5	E	140	17
O7	E	E	25
O6.5	E	E	33
O6	E	E	41
O5.5	E	E	41
O5	E	E	46

NOTES.—Evolution of an H II region around a pair of stars of equal mass. Both stars are accreting mass and growing in spectral type. Relative to Table 2, both the mass and the ionizing flux have been doubled. The numbers in the table indicate the radius of the trapped H II region around the star. The letter Q indicates that the H II region is quenched, meaning that there is no solution for ionization equilibrium because the ionizing flux is too small compared to the accretion rate. The letter E means that the H II region is no longer trapped but expanding. Relative to Table 2, the higher mass and ionizing flux allow the formation of larger trapped H II regions.

as the flux of ionizing photons increases along with the temperature and mass of the star. Tables 2–4 show a few cases illustrating the evolution of an H II region around single and multiple stars.

Tables 2–4 show that depending on the surrounding molecular density, the H II region begins quenched, moves into the stable, long-lived trapped phase, and finally moves beyond the critical radius into the rapid expansion phase. Because stellar growth ends once the H II region enters the expansion phase, the final stellar type is determined entirely by the density of the molecular gas. At higher molecular densities, the star will grow to larger mass because more ionizing radiation is required to move the boundary of the H II region beyond the critical point for expansion.

TABLE 3
EVOLUTION OF H II REGIONS AROUND MULTIPLE STARS

Spectral Type	$n_\infty = 50\ \mathrm{cm}^{-3}$ (AU)	$n_\infty = 75\ \mathrm{cm}^{-3}$ (AU)	$n_\infty = 100\ \mathrm{cm}^{-3}$ (AU)
B0.5	1	Q	Q
B0	5	Q	Q
09.5	20	1	Q
09	57	2	Q
O8.5	101	3	Q
O8	E	6	1
O7.5	E	10	1
O7	E	14	2
O6.5	E	18	2
O6	E	22	2
O5.5	E	22	2
O5	E	25	2

NOTES.—Evolution of an H II region around a group of stars that is accreting mass and growing in spectral type. The calculation assumes that there are a number of later type stars with nonionizing radiation accompanying one massive star. In these examples, the combined mass of the later type stars is set equal to the mass of the early-type star. In other words, relative to Table 2, the mass has been doubled, but the ionizing flux has remained the same. The numbers in the table indicate the radius of the trapped H II region around the star. The letter Q indicates that the H II region is quenched, meaning that there is no solution for ionization equilibrium because the ionizing flux is too small compared to the accretion rate. The letter E means that the H II region is no longer trapped but expanding. Relative to Table 2, the higher total mass allows the formation of individual stars of higher mass in lower densities of molecular gas.

Table 2 illustrates the evolution of H II regions around single stars. In Table 3, the mass due to stars within the H II region has been doubled, as could be caused by a few accompanying later type stars that add mass to the system but do not increase the ionizing flux. (The separation of the group is considered to be small enough that the gravitational potential of the system on the scale of the trapped H II region is still essentially spherical.) With more mass, the critical point of the accretion flow moves outward, and a higher ionizing flux is required to end the evolution. In Table 4, both the stellar mass and the ionizing flux have been doubled, as might be the case, for example, with an equal-mass binary. But because the ionizing flux of a star scales as a high power of its mass, massive stars forming together will have a lower flux-to-mass ratio than a single star of equivalent mass. With a lower flux-to-mass ratio, a group of stars will be able to continue accreting mass longer and will grow to earlier spectral types before their surrounding trapped H II region begins the expansion phase. The trends in the tables show that the conditions that favor the formation of the most massive stars are high densities of molecular gas and formation in binaries or multiplets.

Some caution must be used when interpreting the numbers in the tables. Because the recombination rate scales as the square of the density, and because the density increases rapidly inward asymptotically approaching an $r^{-3/2}$ limit, the densities and the recombination rate become very high near the stellar radius. However, it is possible in real clouds that other effects could limit the increase in density at very small radii. If so, the molecular densities in Tables 2–4 could be higher.

3. EVOLUTION OF THE STARS

Could a massive star of several tens of solar masses, with a main-sequence lifetime on the order of 10^6 yr, accrete sufficient mass before evolving off the main sequence if the accretion rate were as low as those in Table 1 (10^{-5} to 10^{-4} $M_\odot$ yr^{-1})? To estimate the effect of the continuing accretion on the stars powering the trapped H II regions, Alessandro Chieffi (2003, private communication) ran numerical simulations of the pre–main-sequence and main-sequence evolution of stars growing to early types with continuous input of hydrogen at the stellar surface (see Chieffi, Straniero, & Salaris 1995 and Limongi, Straniero, & Chieffi 2000 for the method of simulation). Figure 1 shows three evolutionary tracks of a 1 $M_\odot$ star evolving at accretion rates proportional to the square of the stellar mass (eq. [1]) and values of 0.33, 1.0, and 3.0×10^{-5} $M_\odot$ yr^{-1} at 13 $M_\odot$. Also plotted is the evolution of a 1 $M_\odot$ star evolving to the main sequence without accretion (D'Antona & Mazzitelli 1994). Both stars follow an identical path for some time before the effects of accretion cause a deviation toward increased luminosity. The higher luminosity is the result of the larger radius of the pre–main-sequence star that is, in turn, caused by the burning of fresh deuterium that is continuously supplied by the accretion. The track of the accreting star remains above the main sequence until it has accumulated around 2.5 $M_\odot$. Thereafter, it evolves directly up the zero-age main-sequence (ZAMS) line with increasing luminosity and temperature equivalent to the luminosities and temperatures of nonaccreting ZAMS stars of progressively higher mass (Schaller et al. 1992). The simulation shows that the mass accretion rates in Table 1 supply fresh hydrogen at a sufficient rate to keep the accreting star on the ZAMS line. In other words, the star does not exhaust its supply of hydrogen and remains on the main sequence as long as the accretion continues. Thus, relatively slow accretion is able to build early-type stars of high mass.

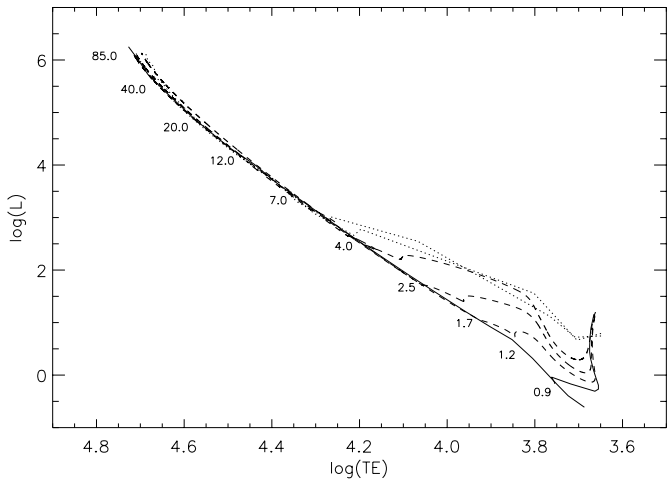

FIG. 1.—H-R diagram for massive stars forming by accretion. The ZAMS line (*solid line*) is from Schaller et al. (1992). The three dashed lines show the tracks of a star accreting mass at three different rates, each proportional to the stellar mass squared, as suggested by the simple model of § 2. The accretion rates are set to 0.33, 1.0, and 3.0×10^{-5} $M_\odot$ yr^{-1} for a stellar mass of 13 $M_\odot$. The evolution starts at 1 $M_\odot$ and initially follows the evolutionary track (*solid line*) of a nonaccreting star (D'Antona & Mazzitelli 1994) before diverging to higher luminosity. The two thin dotted lines (from Norberg & Maeder 2000) show the evolution of stars accreting mass at a higher rate, 10^{-5} $M_\odot$ yr^{-1} for a stellar mass of 1 $M_\odot$, and a rate that increases as the 1.0 and 1.5 power of the stellar mass.

This result is the same as that found earlier by Beech & Mitalas (1994), Bernasconi & Maeder (1996), Meynet & Maeder (2000), Norberg & Maeder (2000), and Behrend & Maeder (2001) for higher accretion rates than those considered in this paper. Two evolutionary tracks given by Norberg & Maeder (2000) are plotted in Figure 1 for comparison. Compared to stars evolving with the lower accretion rates of Table 1, these tracks deviate earlier from the evolutionary track of a nonaccreting 1 $M_\odot$ star and join the main sequence at higher masses. These higher rates would require higher densities in the surrounding molecular gas than those considered in the examples in Tables 1–4. To achieve the rate in Norberg & Maeder (2000) of 10^{-5} $M_\odot$ yr^{-1} onto a 1 $M_\odot$ star would require a density at infinity of 7×10^4 cm^{-3}, which implies a density of 5×10^5 cm^{-3} at the sonic point located at 0.42 pc, assuming a sound speed of 0.46 km s^{-1} ($T = 25$ K). The implied high densities are certainly possible in high-mass star-forming regions, but as illustrated in the tables, single stars in such dense surroundings would have difficulty in ionizing their H II regions beyond the critical radius required to initiate expansion of the H II region and halt the accretion flow. Thus, in such dense cores, one might expect the formation of binaries or small groups of high-mass stars.

Although the evolutionary tracks begin at 1 $M_\odot$, massive stars are not likely to grow from such a low mass by Bondi accretion, because the timescale would be too long. More likely, the collapse of a dense molecular cloud core will result in a star of some higher mass, for example, 10 $M_\odot$, that could then evolve to an earlier spectral type by continuing accretion on a timescale of a million years or so.

4. RADIATION PRESSURE

Pressure on dust grains that absorb the radiation from the star or stars in an H II region and the radiation from any shock at the base of an accretion flow where the flow decelerates can be competitive with the gravitational attraction of the stars (Mestel 1954; Larson & Starrfield 1971; Appenzeller & Tscharnuter 1974; Kahn 1974; Yorke & Krugel 1977; Wolfire & Cassinelli 1987) One can derive a limiting luminosity-to-mass ratio by balancing the outward force of the radiation against the inward force of gravity,

$$\frac{L}{M} = \frac{4\pi c G}{\kappa} .$$

Assuming an extinction coefficient for interstellar dust, $\kappa \sim 100$ cm^2 g^{-1} (Mathis, Rumpl, & Nordsieck 1977), the maximum luminosity-to-mass ratio is about 2500 $L_\odot/M_\odot$, a value that would be exceeded by an early B-type star. From this simple argument, it would seem impossible to form a massive star by accretion.

However, this simple argument may not be correct. Kahn (1974) and Wolfire & Casinelli (1986, 1987) have pointed out that the stellar radiation is absorbed in a thin boundary layer that is found at the point in the accretion flow where the gas temperature, which is increasing as the flow approaches the star, reaches the sublimation temperature of the dust. In front of this layer, the dust will be sublimated and therefore not available to absorb the stellar radiation. Behind this boundary layer, the radiation field that is

reemitted by the dust will have the temperature of the dust, not the star, and the radiation will be mostly in the infrared. Because the opacity of the dust at infrared wavelengths is orders of magnitude lower than at optical and shorter wavelengths (Krugel & Siebenmorgan 1994), the transfer of momentum from the radiation to the dust will be much lower. Thus, for most of the cloud, except within the absorbing boundary layer, the infrared radiation passes through the cloud without exerting much pressure on the dust. At the boundary layer, where the radiation temperature is the same as the stellar photospheric temperature, the opacity of the dust is high, and the dust will absorb the full pressure of the radiation. However, because the boundary layer is thin, it is possible for the momentum of the accretion flow to push the gas and dust through this boundary layer into the sublimation zone, where the dust is destroyed. This requires that the momentum of the flow $\dot{M}v$ must be higher than the momentum of the radiation given by the ratio of the luminosity of the flow and the speed of light, L/C.

The minimum momentum required to overcome the radiation pressure may be estimated if we know the radius at which the dust sublimates and the velocity of the accretion flow at that radius. The sublimation radius of the dust in a continuing accretion flow may be assumed to be the ionization boundary of the H II region. The accretion flow speed is then given by the Bernouilli equation for the molecular gas. The minimum speed of the molecular flow at the boundary of a trapped H II region will be found when the H II region has reached its maximum trapped radius, approximately at the sonic point of the ionized flow. At this radius, the molecular gas has an infall velocity that is always twice the sound speed of the ionized gas, and the minimum momentum of the accretion flow onto an H II region in the trapped phase is the flow rate times twice the sound speed of the ionized gas, $\dot{M}2c_2$.

Figure 2 compares the momentum of the radiation with the momentum of the flow for different stellar masses. The minimum accretion rate for the HC H II model is $\dot{M} > L/C2c_2$. The maximum rate in Figure 2 is the Eddington luminosity, as a function of mass, where the absorption is due to classical electron scattering. The minimum and maximum accretion rates to overcome the radiation pressure in the trapped HC H II model bracket the accretion rates suggested in this paper, as well as the higher rate suggested by Norberg & Maeder (2000). The minimum accretion rate suggested by Wolfire & Cassinelli (1987) is also plotted and appears just below the minimum rate for the HC H II regions. The two estimates are almost the same, except that the sublimation radius of Wolfire & Cassinelli (1987), their equation (18), is calculated from more complex considerations of the molecular gas temperature around massive stars versus the sublimation temperature of grains, whereas the sublimation radius for continuing accretion is simply the ionization boundary of the H II region. The trend shown in Figure 2 illustrates that the accretion rate must increase as some power of the stellar mass in the range of $\frac{1}{2}$ to 2 in order to overcome the radiation pressure and form stars of the highest mass.

While the accretion flows considered in this paper are restricted to spherical geometries to simplify the analysis, other studies that consider radiation pressure in nonspherical flows suggest that the effect on the inflowing gas is less than in spherical geometries (Nakano 1989; Nakano, Hasegawa, & Norman 1995; Jijina & Adams 1996).

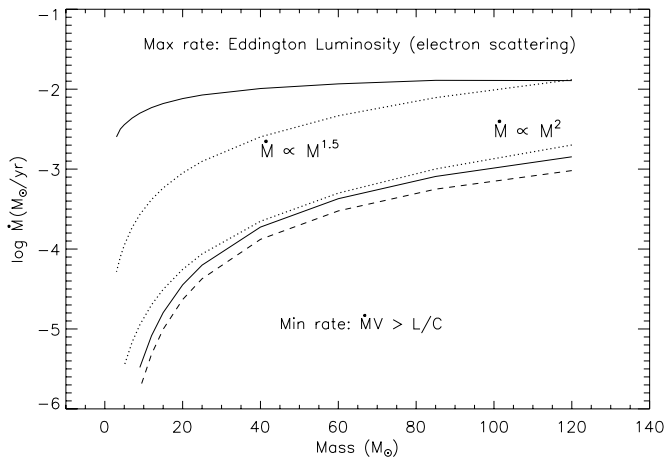

FIG. 2.—Minimum and maximum accretion rates (*solid lines*) allowed by the radiation of a high-mass star and accretion shock. The lower limit is set by the requirement that the inward momentum of the accretion flow exceed the outward momentum of the radiation from the star and accretion shock. The upper limit on the accretion rate is set by the requirement that the luminosity of the star and shock be less than the Eddington luminosity of the star. The numerical value for the cross section for electron scattering is taken from Lamers (1986). An accretion rate suggested in this paper of 4.7×10^{-5} $M_\odot$ yr^{-1} for an 18 $M_\odot$ star, scaling as M^2, and an accretion rate suggested by Norberg & Maeder (2000), 10^{-5} $M_\odot$ yr^{-1} for a 1 $M_\odot$ star, scaling as $M^{1.5}$ (*dotted lines*), both fall within the allowed region. Also plotted for reference is the minimum accretion rate suggested by Wolfire & Cassinelli (1987; *dashed line*).

5. OBSERVATIONAL PROPERTIES OF THE HYPERCOMPACT H II REGIONS

The trapped HC H II regions have a specific density structure, and it is possible to predict their observational characteristics. Because they will be found deeply embedded in the dense molecular gas of massive star-forming regions, they will only be observable at long wavelengths from infrared to radio. Using some approximations, it is possible to model the radio continuum emission of the trapped HC H II regions with very simple equations.

5.1. *Approximate Densities and Velocities*

The exact density profiles of the molecular and ionized gas in a spherically symmetric accretion flow through a trapped H II region are found by solving the nonlinear Bernouilli equation for the energy of the accretion flow (eqs. [4] and [12] in K02b). However, because the accretion flows are dominated by gravity at radii less than the sonic point, $r_s = GM/2c^2$, and by pressure at larger radii, approximate densities can be obtained by using the free-fall density profile inside the sonic point and the equation of hydrostatic equilibrium outside the sonic point. If n_{r_s} is the density at the sonic point, then at smaller radii

$$n(r) \approx n_{r_s}(r_s/r)^{1.5} , \tag{3}$$

and at larger radii

$$n(r) \approx n_{r_s} \exp\left[-2\left(1 - \frac{r_s}{r}\right)\right] . \tag{4}$$

(The hydrostatic equation appears different from that in planetary atmospheres, because here the gravitational force varies with radius as $1/r$ and is not assumed to be constant.) With these approximations, the errors in density at 1/2,

1/10, and 1/100 times the sonic radius are 33%, 80%, and 190%, respectively. On the outside, at distances of 2, 3, and 4 times the sonic radius, the errors are 32%, 37%, and 39%, respectively. Thus, if the sonic point for a molecular accretion flow is located at 0.1 pc, then over a range of radii 0.001–0.4 pc the approximations are good to within a factor of 2. The density at infinity that appears in the scaling for the theoretical formulas is approximately e^{-2} times the density at the sonic point.

A slightly better approximation to the density profile at smaller radii can be obtained by multiplying the approximate density by $\sqrt{2}$. This factor partially compensates for the discrepancy between the approximate and exact solutions near the sonic point, where the flow is still making a transition from hydrostatic to free fall. Just inside the sonic point, the approximate power-law solution initially falls off too fast before becoming an excellent approximation, and thus the correct densities are slightly higher than the approximate densities throughout the H II region. The factor of $\sqrt{2}$ is arbitrary, but over the size scales appropriate for the trapped H II regions, it is an improvement.

Since the accretion flow is steady state, the velocity at any point in the accretion flow can be found from the density profile using the equation of conservation and the fact that, by definition, the velocity at the sonic point is the sound speed

$$v(r) = \frac{r_s^2 n_{r_s} c}{r^2 n(r)} \ . \tag{5}$$

These estimates suffice for the flows that are entirely within the ionized or molecular zones separately. For the complete flow across the ionization boundary, it is possible to derive a simple approximate solution for the case in which the boundary is at the sonic point of the ionized flow. At the maximum radius of an H II region in the trapped phase, because the sonic point is so close to the critical point, it is possible to ignore the shock front that has already begun to separate from the ionization front and treat the H II boundary as a simple stationary ionization front with an *R*-critical jump (§ 3.2 of K02b). In an *R*-critical jump, the velocity of the ionized gas leaving the front will be equal to its sound speed. Knowing the velocity of both the ionized and molecular flows on either side of the boundary and knowing the density of the molecular gas, it is possible to derive the density of the ionized gas from the jump condition:

$$\rho_1 v_1 = \rho_2 v_2 \ . \tag{6}$$

Continuing the approximations, it is also possible to determine the ionizing flux in equilibrium with the recombination rate within the H II region, using the equation for the radius of a Strömgren sphere (Spitzer 1978; or eq. [13] of K02b),

$$N_i = 4\pi \int_{r_*}^{r_s} n^2 \alpha r^2 \, dr \ , \tag{7}$$

but with a –3/2 power-law density profile, rather than the constant density of the traditional Strömgren sphere. With $n \sim r^{-3/2}$,

$$N_i = 4\pi r_s^3 n_{r_s}^2 \alpha [\ln(r_s) - \ln(r_*)] \ . \tag{8}$$

Here α is the recombination rate, about 3×10^{13} cm^{-3} s^{-1}, and r_* is the stellar radius. For the trapped H II regions considered in this paper, the error in this approximation of the ionizing flux is about 50%.

As an example, consider a 40 $M_\odot$ star with molecular and ionized gas temperatures of 25 K (Wolfire & Churchwell 1994) and 10,000 K. The sound speeds, c_1 and c_2 are then 0.46 and 12.9 km s^{-1}, and the sonic points of the two flows are at $r_{s1} = 0.42$ pc and $r_{s2} = 107$ AU. Further assume a molecular gas density of 740 cm^{-3} at r_{s1}. (This implies a number density at infinity that is about a factor of e^{-2} less, or about 100 cm^{-3}.) Since we know the molecular velocities at r_{s1} and r_{s2}, it is better to calculate the number density using the conservation law than the other way around. The number density of the molecular gas at r_{s2} is $n(r_{s2}) = c_1 n_1 r_{s1}^2 / 2 c_2 r_{s2}^2 = 8.6 \times 10^6$ cm^{-3}. Since the velocity of the ionized gas at the back of the *R*-critical front at r_{s2} is the sound speed, the jump condition, $2 n_1 v_1 = n_2 v_2$, yields the density of the ionized gas at r_{s2}, $n(r_{s2}) = 3.4 \times 10^7$ cm^{-3}. (The factor of 2 in the jump condition assumes that the neutral gas is composed of molecular hydrogen.) The flux of ionizing photons required for photoionization equilibrium is then $N_i = 3 \times 10^{49}$, equivalent to the flux of an O5 star, assuming a stellar radius of 11.8 $R_\odot$.

6. RADIO EMISSION OF OPTICALLY THICK H II REGIONS

Observational studies have detected compact sources of weak radio continuum emission from the dense molecular cloud cores that are thought to be the sites of massive star formation. The compact radio continuum emission is weaker than would be expected from optically thin ultracompact (UC) H II regions, and its origin is not understood. Several possible explanations have been suggested: dust in the H II regions may be absorbing ionizing photons; the ionizing stars may not have reached the main sequence; the ionization may derive from a cluster of less massive stars; the H II regions may be optically thick (Wood & Churchwell 1989b; Kurtz, Churchwell, & Wood 1994; Garay et al. 1993; Keto et al. 1994; Miralles, Rodríguez, & Scalise 1994; Garay & Lizano 1999; Carral et al. 1999, Molinari et al. 1998). Because of their steep density gradients, the HC H II regions will always be optically thick through their central regions, and their free-free emission could be the observed weak continuum. Using the models of § 2 for the trapped HC H II regions, the characteristics of the free-free emission from the dense ionized gas in these sources can be predicted. The radio free-free emission of a spherical H II region seen as an unresolved source is

$$S_\nu = 4\pi k T_e \nu^2 / c^2 \int_0^{\theta_0} \theta \left[1 - e^{-\tau_\nu}\right] d\theta \ . \tag{9}$$

Here θ is an angular coordinate on the plane of the sky,

$$\theta = \sqrt{x^2 + y^2} / D \ ,$$

where coordinate axes x and y are centered on the H II region, $\theta_0 = R_0 / D$, R_0 is the radius of the H II region, and D the distance to the source. An approximation to the free-free optical depth is given by Altenhoff, Strittmatter, & Wendker (1981) or equation (A.1a) of Mezger & Henderson (1967),

$$\tau_\nu = 8.235 \times 10^{-2} \left(\frac{T_e}{\mathrm{K}}\right)^{-1.35} \left(\frac{\nu}{\mathrm{GHz}}\right)^{-2.1} \left(\frac{\mathrm{EM}}{\mathrm{pc\ cm^{-6}}}\right) \ , \tag{10}$$

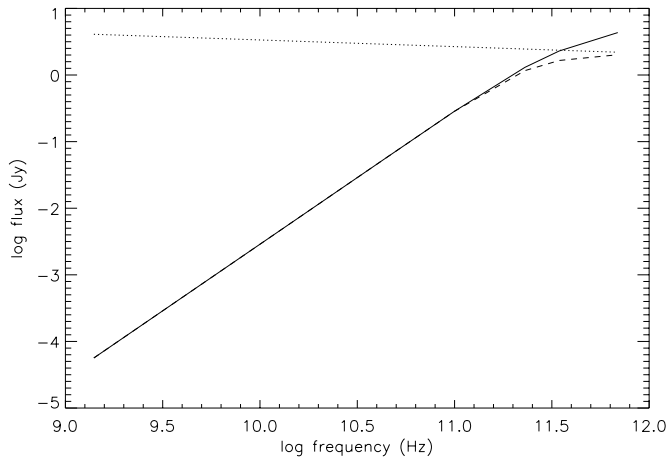

FIG. 3.—Predicted spectral index of an HC H II region with radius of 107 AU and an ionized density at the boundary of 2.5×10^7 cm^{-3}. This ionized gas density would be consistent with a molecular gas density at the boundary of 6.4×10^5 cm^{-3} and a molecular density of 2.1×10^4 cm^{-3} at 0.1 pc. The solid line shows the spectral index for an H II region with an $r^{-3/2}$ density gradient, and the dashed line shows the spectral index for an H II region with constant density. Both H II regions are optically thick at all but the highest frequencies. The dotted line shows the predicted flux using the optically thin approximation.

where T_e is the electron temperature and EM is the emission measure, $n_e^2 L$.

Figures 3, 4, and 5 show the radio continuum emission as a function of frequency for three H II regions of 107 AU with different densities. For the gas density used in Figure 3, the flux of ionizing photons required for equilibrium is $10^{49.3}$ s^{-1} and could be produced by a single O6 star whose mass would be about 40 $M_\odot$ (Vacca, Garmany, & Shull 1996). Since the recombination rate scales as the square of the density, the number of ionizing photons for the models of Figures 4 and 5 are factors of 10^2 and 10^4 less than the equilibrium flux of $10^{49.3}$ s^{-1} of Figure 3. The flux of Figure 5 is quite low, but correspondingly, the molecular density, 10^3 cm^{-3}, consistent with the ionized density of the model in Figure 5, is less than expected in a massive star-forming region. Also plotted for comparison is the free-free radio emission that the H II region would have if it had a constant

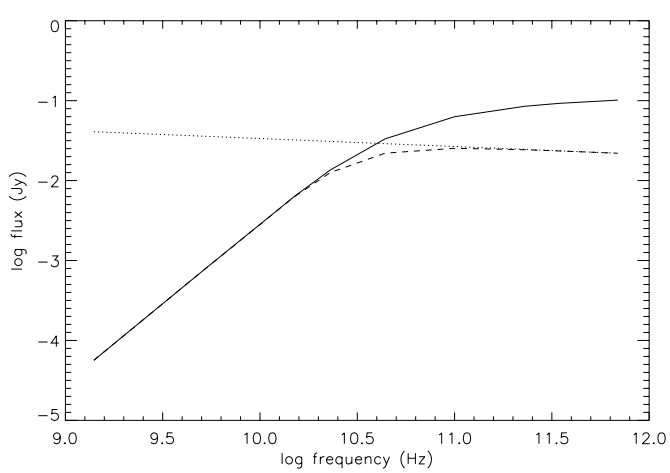

FIG. 4.—Predicted spectral index of an HC H II region with radius of 107 AU and an ionized density at the boundary of 2.5×10^6 cm^{-3}, in the same format as Fig. 3.

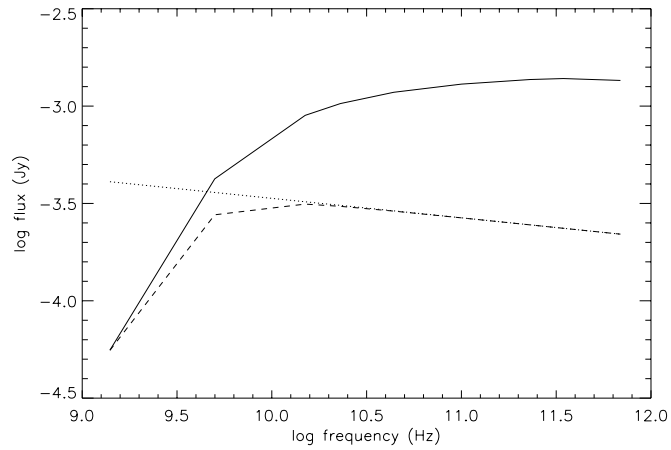

FIG. 5.—Predicted spectral index of an HC H II region with radius of 107 AU and an ionized density at the boundary of 2.5×10^5 cm^{-3}, in the same format as Fig. 3.

density. The spectral indices of the two cases show that the trapped H II regions appear
optically thick at lower frequencies because of the higher densities in their interiors. If one were to derive the electron density from the continuum emission using assumptions of constant density and optically thin emission, the constant density assumption would overestimate the electron density, while the optically thin assumption would underestimate. A better procedure is outlined in the next section.

6.1. *Approximate Fluxes for Partially Thick* H II *Regions*

If a spherical H II region has a power-law density gradient, then it will always be optically thin along lines of sight, with large impact parameters that have shorter path lengths and that pass through lower density gas. Conversely, it will always be optically thick along lines of sight close enough to the center. The flux from such a partially optically thick H II region can be estimated by using the optically thin approximation on lines of sight at large impact parameters, where the optical depth is less than unity, and the optically thick approximation on lines of sight near the center. The approximate formulas provide an easy way to predict the radio continuum emission from the trapped HC H II regions.

In the optically thin approximation, the brightness temperature is proportional to the emission measure along the line of sight. In a spherical H II region, a line of sight at impact parameter, b, will have an emission measure

$$\mathrm{EM}(b) = 2\int_0^{Z_0} n_e^2(r)\,dz\ , \tag{11}$$

where $Z_0^2 = R_0^2 - b^2$, R_0 is the radius of the H II region, and $2Z_0$ is then the path length or chord along the line of sight at impact parameter b. The Cartesian axes x, y, and z have their origin at the center of the H II region, with z along the line of sight and x and y in the plane of the sky. If the electron density is $n(r) = n_0(R_0/r)^{3/2}$, with n_0 being the density at the H II region boundary, the emission measure is then

$$\mathrm{EM}(b) = 2R_0^3 n_0^2 \int_0^{Z_0} (b^2 + z^2)^{-3/2}\,dz\ , \tag{12}$$

which evaluates to

$$\mathrm{EM}(b) = 2R_0^3 n_0^2 \frac{Z_0}{b^2(b^2+Z_0^2)^{1/2}} \ . \tag{13}$$

Switching to angular coordinates, θ, where D is the distance to the source,

$$\theta = b/D \ ,$$

$$\theta_0 = R_0/D \ ,$$

$$\mathrm{EM}(\theta) = 2Dn_0^2 \frac{\theta_0^2}{\theta^2}\sqrt{\theta_0^2-\theta^2} \ . \tag{14}$$

For optically thin emission, the brightness along the line of sight is directly proportional to the emission measure (eq. [6] of Mezger & Henderson 1967),

$$T_b(\theta) = A_{\mathrm{FF}}\ \mathrm{EM}(\theta) \ . \tag{15}$$

The factor A_{FF}, assuming that the emission measure is in units of pc cm^{-6}, is

$$A_{\mathrm{FF}} = 8.235\times 10^{-2} T_e^{-0.35}\left(\frac{\nu}{\mathrm{GHz}}\right)^{-2.1} \ . \tag{16}$$

For optically thick emission, the brightness temperature is simply equal to the gas temperature.

The antenna temperature of an ideal antenna (assuming uniform illumination and ignoring inefficiency) is

$$T_A = \frac{1}{\Omega}2\pi\int_0^{\theta_0}\theta T_b(\theta)\,d\theta \ , \tag{17}$$

where Ω is the solid angle subtended by the source. If θ_1 is the impact parameter at which the optical depth along a line of sight is unity, then using the equation for optically thin emission for the contribution to the antenna temperature from the part of the H II region exterior to θ_1,

$$T_A^{\mathrm{thin}} = A_{\mathrm{FF}}\ \frac{1}{\Omega}2\pi\int_{\theta_1}^{\theta_0} 2Dn_0^2\ \frac{\theta_0^2}{\theta}\sqrt{\theta_0^2-\theta^2} \ , \tag{18}$$

which evaluates to

$$T_A^{\mathrm{thin}} = -4A_{\mathrm{FF}}\ Dn_0^2\left(u+\frac{\theta_0}{2}\ln\frac{\theta_0-u}{\theta_0+u}\right) \ , \tag{19}$$

where

$$u = \sqrt{\theta_0^2-\theta_1^2}.$$

The contribution to the antenna temperature from the thick part of the disk, $\theta < \theta_1$, using the equation for optically thick emission, is

$$T_A^{\mathrm{thick}} = \frac{1}{\Omega}2\pi\int_0^{\theta_1} T_e\,d\theta \ , \tag{20}$$

which evaluates to

$$T_A^{\mathrm{thick}} = \frac{\theta_1^2}{\theta_0^2}\ T_e \ . \tag{21}$$

The antenna temperature for the whole H II region may be approximated as

$$T_A = T_A^{\mathrm{thin}} + T_A^{\mathrm{thick}} \ , \tag{22}$$

or in terms of flux density,

$$S_\nu = 2kT_A\Omega c^2/\nu^2 \ . \tag{23}$$

The value of θ_1 can be determined from the equation for the optical depth of the free-free emission,

$$\tau_\nu(\theta) = A_{\mathrm{FF}}/T_e 2Dn_0^2\ \frac{\theta_0^2}{\theta^2}\sqrt{\theta_0^2-\theta^2} \ . \tag{24}$$

With $\tau_\nu = 1$, the solution is

$$\theta_1^2 = 2(A_{\mathrm{FF}}Dn_0^2)^2\left[-1+\sqrt{1+\theta_0^2(A_{\mathrm{FF}}Dn_0^2)^{-2}}\right] \ . \tag{25}$$

Table 5 lists fluxes determined by both this approximate method with the approximate density profile of § 2.1 and numerical calculation using the exact density profile as given by the Bernouilli equation. The example H II region in

TABLE 5

RADIO CONTINUUM FLUX OF THE TRAPPED HC H II REGIONS

Frequency (GHz)	$r(\tau=1)$ Exact[a] (AU)	$r(\tau=1)$ Approx.[b] (AU)	Exact Flux[a] (mJy)	Approx. Flux[c] (mJy)	Thin Flux[d] (mJy)
1.4	107.0[e]	107.0	0.06	0.06	256
5.0	107.0	107.0	0.7	0.7	226
15.0	105.9	103.5	6	9	202
23.0	101.6	92.8	13	19	194
44.0	71.7	60.5	33	42	182
100.0	26.7	27.7	63	64	167
230.0	9.6	11.7	85	91	154
345.0	5.9	7.7	93	102	148
690.0	2.7	3.7	102	138	120

[a] Calculated numerically using the density profile as given by the solution of the Bernouilli equation.

[b] Radius where $\tau = 1$ using approximate method of § 5.1.

[c] The approximate fluxes using the approximate model for trapped HC H II region, as described in § 2.1, and the approximate formula for the flux, as described in § 5.1. The ionized gas densities include the $\sqrt{2}$ correction.

[d] Flux calculated using the optically thin approximation.

[e] At low frequencies the H II region is essentially optically thick everywhere.

Table 5 has the same structure as that used to compute the fluxes in Figure 3. Table 5 shows that the approximation is correct to within 35%, whereas the optically thin approximation, also shown in the table, is off by orders of magnitude when the emission is partially optically thick. Thus, derivations of the electron density and the number of ionizing photons in small H II regions with steep density gradients may be in error, if the emission measure is determined using the optically thin approximation over the entire H II region.

7. BROAD RADIO RECOMBINATION LINES

Radio recombination lines observed in HC H II regions tend to be broader (50–180 km s^{-1}) than those observed in typical UC H II regions (30 km s^{-1}) (Altenhoff et al. 1981; Zijlstra et al. 1990; Keto et al. 1995; Gaume, Fey, & Claussen 1994; Depree et al. 1994, 1996, 1997; Jaffe & Martín-Pintado 1999; K02a). The large line widths have generally been interpreted as evidence for high-velocity outflows. This is certainly the case for some H II regions, but the model for continuing accretion offers another interpretation applicable to those H II regions that are in the trapped phase. In the trapped HC H II regions, the large recombination line widths are due to a combination of pressure broadening and high infall velocities in the steep density gradients and accelerating accretion flows through the trapped H II regions.

The lowest infall velocity in the ionized gas of a trapped H II region is the sound speed, and the ionized accretion flow will attain this velocity at the ionization boundary when the H II region is at its maximum trapped size. At smaller radii and for smaller H II regions, the velocity scales inward as approximately $r^{-1/2}$. Thus, infall velocities of many times the sound speed are realizable. The ratio of pressure broadening to thermal broadening scales linearly with the electron density and as the seventh power of principal quantum number of the recombination line. At centimeter wavelengths the pressure broadening is equivalent to the thermal line width at densities as low as 10^5 cm^{-3} (Keto et al. 1995),

$$\frac{\Delta\nu_p}{\Delta\nu_{\rm th}} = 1.2\frac{n_e}{10^5\ {\rm cm}^{-3}}\left(\frac{N}{92}\right)^7 .$$

As the density increases inward even more steeply than the velocity, pressure-broadened widths of many times the sound speed are to be expected in HC H II regions.

An interesting correlation between the spectral index of the free-free radio continuum and the line width of the H66α was noted in the HC H II regions in the W49A star-forming region (Depree et al. 1997). This correlation would be expected if the recombination line widths had a component due to pressure broadening, since both pressure broadening and the spectral index are higher for high-density gas. A lack of correlation between line width and electron density is also expected if the electron densities are calculated assuming constant density and optically thin emission, while the H II regions do not meet these assumptions because of steep density gradients.

8. THE LIFETIMES OF UC H II REGION

An H II region in the classical model for pressure-driven evolution expands at approximately the sound speed of the ionized gas, and the age of an expanding H II region is approximately equal to its radius divided by the sound speed. Expanding UC H II regions observed to have radii less than 0.1 pc would then have dynamical ages of a few thousand years. Such short ages are inconsistent with observations. Because the gravitationally trapped H II regions have much longer lifetimes, they potentially resolve a number of these observational problems. However, not all H II regions are gravitationally trapped, and this model will not be appropriate for many observed H II regions. In particular, H II regions with cometary or arc-shaped morphologies are likely to be rapid outflows, "champagne" flows, down steep density gradients in the surrounding molecular gas (Tenorio-Tagle 1979; Franco, Tenorio-Tagle & Bodenheimer 1990; Keto et al. 1995; Shu et al. 2002). H II regions with irregular or shell-like morphologies are not well explained but are unlikely candidates for trapping.

8.1. *The Embedded Population*

The number of H II regions in the galaxy has been estimated by Wood & Churchwell (1989a, 1989b), who identified embedded H II regions by a combination of characteristic infrared colors and fluxes in the *IRAS* database (infrared luminosities greater than 10^4 $L_\odot$ and colors 25 μm/12 μm > 3.7 and 60 μm/12 μm > 19.3). They found 1717 such sources and, by comparison to the population of visible O stars, determined that O stars spend 10%–20% of their lifetime deeply embedded in the molecular clouds. This implies a lifetime for the embedded phase of 10^5 yr or more, incompatible with the 10^3 yr dynamical timescale of a pressure-driven H II region, but consistent with the expected timescale of a trapped HC H II region that is slowly growing on an accretion timescale. Many of the Wood & Churchwell *IRAS* sources may be embedded, trapped HC H II regions.

8.2. *Timescales for Formation in Clusters*

Continuum observations of massive star-forming regions often show clusters of UC H II regions, many with size scales of 0.01–0.1 pc. The dynamical ages of these H II regions in pressure-driven expansion of 10^3–10^4 yr are significantly shorter than the gravitational free-fall time (10^5 yr) for molecular gas with a density typical of massive star-forming regions of 10^5 cm^{-3}. The short ages implied by the model for pressure-driven expansion raise the question of how the stars powering these H II regions could have formed simultaneously with a spread in age that is only a fraction of the free-fall time of the host molecular core (Ho, Klein, & Haschick 1987). The gravitationally trapped HC H II regions resolve this problem because their lifetimes are tied directly to the accretion timescale of the stars.

8.3. *Timescales for Expansion in Clusters*

The presence of multiple UC H II regions in clusters indicates that most of the individual H II regions in a cluster cannot be rapidly expanding. Some of these UC H II regions, despite their relatively large sizes, may be gravitationally trapped by a small group of stars. For example, an H II region that has a size of 0.01 pc could be trapped by a total stellar mass of 800 $M_\odot$. The H II region G10.6–0.4 (K02a) is an example of a UC H II region gravitationally trapped by a small group of stars whose combined mass totals several hundred $M_\odot$. In other cases, what appears to be a UC H II region may really be an unresolved group of HC H II regions, each of which is small enough to be trapped by a

single star or binary. These individual HC H II regions only become distinct when viewed at sufficiently high angular resolution. Examples in the literature include the massive star-forming clusters Sgr B2 (Gaume et al. 1995) and W49 (Depree et al. 1997). Figures 1, 2, and 4 in Gaume et al. (1995) show that in Sgr B2, a few UC H II regions with apparent diameters of 0.1–0.2 pc seen in a centimeter continuum image at an angular resolution of 2″.5 pc are resolved into about 50 HC H II regions with sizes less than 5000 AU when observed at 10 times better resolution. Furthermore, the individual H II regions seen at the higher angular resolution may themselves be composed of still smaller H II regions. The kiloparsec distances of most massive star-forming regions makes it difficult to determine the true size scales of the individual H II regions in a cluster.

9. H II REGIONS THAT ARE NOT TRAPPED

HC and UC H II regions may, in general, be in a variety of dynamical states. For example, Tables 2–4 illustrate that the state of an H II region depends sensitively on the density of the surrounding molecular gas, but this model is predicated on a particular and idealized density profile that will not be found in real molecular cores. If a massive star forms in a molecular core that, for whatever reason, has a density gradient steeper than $r^{-3/2}$, ionization equilibrium is not possible (Franco et al. 1990), and a continuous-gradient version of the champagne outflow will result (Tenorio-Tagle 1979; Keto et al. 1995; Shu et al. 2002; Lizano et al. 2003). Thus, not all HC H II will go through a trapped phase. Conversely, the trapped phase is not necessarily restricted to HC H II regions. Trapped UC H II regions may form around a tight cluster of early stars whose combined mass is sufficient to establish a sonic point relatively far from the cluster (K02a).

The morphology of an H II region can offer some guidance to the dynamical state. For example, H II regions that are cometary or shell-like in shape are unlikely to be trapped. The cometary morphology is suggestive of expansion down a steep density gradient, while the shell morphology implies a density structure that is the result of other outward forces, such as stellar winds. However, the dynamics within or outside a trapped H II region need not be strictly symmetric, because the confinement due to the gravitational force of the stars is inherently hydrodynamically stable. For example, because of this stability, it should be possible for a trapped H II region to coexist with other phenomena, such as an accretion disk or bipolar outflow. Nevertheless, the most likely morphology of a trapped H II region would be roughly spherical and centrally bright.

10. CONCLUSIONS

It is possible to form high-mass stars by accretion, despite the thermal and radiation pressure created by the radiation of the high-mass stars and the radiation from the shock at the base of the star-forming accretion flow. Accretion can continue past the time of formation of an H II region around a newly formed star if the equilibrium radius of ionization is small enough that the escape velocity from the star exceeds the sound speed of the ionized gas at the H II region boundary. Radiation pressure will not reverse a star-forming accretion flow if the momentum of the flow at the H II region boundary exceeds the momentum of the radiation. In this case, the dust grains are pushed through the ionization boundary and sublimated.

ZAMS stars within the trapped H II regions may grow to higher masses and earlier spectral types by continuing accretion through the H II region. The evolutionary path of the accreting stars follows directly up the ZAMS line.

The final mass that a star attains within a trapped H II region will depend on the density of the surrounding molecular gas. The conditions that favor the formation of the most massive stars are high densities in the surrounding molecular gas and formation with one or more partners in a binary or multiplet.

The radio free-free emission of the trapped HC H II regions will always be optically thick through the center of the H II region. High optical depth and small size ensure that the radio emission will be relatively weak.

A newly formed H II region cannot expand hydrodynamically if the ionization boundary is less than the distance from the star where the escape velocity equals the sound speed of the ionized gas. The long-lived, gravitationally trapped phase addresses the difficulties imposed by the model for the pressure-driven expansion of H II regions that predicts impossibly short lifetimes for HC and UC H II regions.

REFERENCES

Altenhoff, W., Strittmatter, P., & Wendker, H. 1981, A&A, 93, 48
Appenzeller, I., & Tscharnuter, W. 1974, A&A, 30, 423
Beech, M., & Mitalas, R. 1994, ApJS, 95, 517
Behrend, A., & Maeder, A. 2001, A&A, 373, 190
Bernasconi, P., & Maeder, A. 1996, A&A, 307, 829
Bondi, M. 1952, MNRAS, 112, 195
Carral, P., Kurtz, S., Rodríguez, L., Martí, J., Lizano, S., & Osorio, M. 1999, Rev. Mexicana Astron. Astrofis., 35, 97
Chieffi, A., Straniero, O., & Salaris, M. 1995, ApJ, 445, L39
D'Antona, F., & Mazzitelli, I. 1994, ApJS, 90, 467
Depree, C., Gaume, R., Goss, W., & Claussen, M. 1996, ApJ, 464, 788
Depree, C., Goss, W., Palmer, P., & Rubin, R.. 1994, ApJ, 428, 670
Depree, C., Mehringer, D., & Goss, W. 1997, ApJ, 482, 307
Dyson, J., & Williams, D. 1980, The Physics of the Interstellar Medium (New York: Wiley)
Franco, J., Tenorio-Tagle, G., & Bodenheimer, P. 1990, ApJ, 349, 126
Garay, G., & Lizano, S. 1999, PASP, 111, 1049
Garay, G., Rodríguez, L., Moran, J., & Churchwell, E. 1993, ApJ, 418, 368
Gaume, R., Claussen, M., dePree, C., Goss, W., & Mehringer, D. 1995, ApJ, 449, 663
Gaume, R., Fey, A., & Claussen, M. 1994, ApJ, 432, 648
Ho, P., Klein, R., & Haschick, A. 1986, ApJ, 305, 714
Jaffe, D., & Martín-Pintado, J. 1999, ApJ, 520, 162
Jijina, J., & Adams, F. 1996, ApJ, 462, 874
Kahn, F. 1974, A&A, 37, 149
Keto, E. 2002a, ApJ, 568, 754 (K02a)
———. 2002b, ApJ, 580, 980 (K02b)
Keto, E., Proctor, D., Ball, R., Arens, J., & Jernigen, G. 1992, ApJ, 401, L113
Keto, E., Welch, W., Reid, M., & Ho, P. 1995, ApJ, 444, 765
Krugel, E., & Siebenmorgan, R. 1994, A&A, 288, 929
Kurtz, S., Churchwell, E., & Wood, D. 1994, ApJS, 91, 659
Lamers, H. 1986, A&A, 159, 90
Larson, R., & Starrfield, S. 1971, A&A, 13, 190
Limongi, M., Straniero, O., & Chieffi, A. 2000, ApJS, 129, 625
Lizano, S., Galli, D., Shu, F., & Canto, J. 2003, in Rev. Mexicana Astron. Astrofis. Ser. Conf. 15, ed. S. J. Arthur & W. J. Henney (Mexcio, DF: Inst. Astron., UNAM), 166
Mathis, J., Rumpl, W., & Nordsieck, K. 1977, ApJ, 217, 425
Mestel, L. 1954, MNRAS, 114, 437
Meynet, G., & Maeder, A. 2000, A&A, 361, 101
Mezger, P., & Henderson, A. 1967, ApJ, 147, 471
Miralles, M., Rodríguez, L., & Scalise, E. 1994, ApJS, 92, 173
Molinari, S., Brand, J., Cesaroni, R., Palla, F., & Palumbo, G. 1998, A&A, 336, 339
Nakano, T. 1989, ApJ, 345, 464
Nakano, T., Hasegawa, T., & Norman, C. 1995, ApJ, 450, 183
Norberg, P., & Maeder, A. 2000, A&A, 359, 1025

Schaller, G., Schaerer, D., Meynet, G., & Maeder, A. 1992, A&AS, 96, 269
Shu, F. 1992, The Physics of Astrophysics, Volume II, Gas Dynamics (Mill Valley: University Science Books)
Shu, F., Lizano, S., Galli, D., Canto, J., & Laughlin, G. 2002, ApJ, 580, 969
Spitzer, L., Jr. 1978, Physical Processes in the Interstellar Medium (New York: Wiley)
Tenorio-Tagle, G. 1979, A&A, 71, 59
Vacca, W., Garmany, C., & Shull, J. 1996, ApJ, 460, 914
Walmsley, M. 1995, in Rev. Mexicana Astron. Astrofis. Ser. Conf. 1, Circumstellar Disks, Outlaws, and Star Formation, ed. S. Lizano & J. M. Torelles (Mexico, DF: Inst. Astron., UNAM), 137
Wolfire, M., & Cassinelli, J. P.1986, ApJ, 310, 207
Wolfire, M., & Cassinelli, J. P. 1987, ApJ, 319, 850
Wolfire, M., & Churchwell, E. 1994, ApJ, 427, 889
Wood, D., & Churchwell, E. 1989a, ApJS, 69, 831
Wood, D., & Churchwell, E. 1989b, ApJ, 340, 265
Yorke, H. 1984, in Proc. Workshop on Star Formation, ed. R. D. Wolstencroft (Edinburgh: Royal Obs.), 63
———. 2001, ASP Conf. Ser. 267, Hot Star Workshop III: The Earliest Stages of Massive Star Birth, ed. P. A. Crowther (San Francisco: ASP), 165
Yorke, H., & Krugel, E. 1977, A&A, 54, 183
Zijlstra, A., Pottasch, S., Engels, D., Roelfsma, P., te Lintel Hekkert, P., & Umana, G. 1990, MNRAS, 246, 217

The Astrophysical Journal, 635:1370–1372, 2005 December 20
© 2005. The American Astronomical Society. All rights reserved. Printed in U.S.A.

ERRATUM: "THE HUBBLE HIGHER z SUPERNOVA SEARCH: SUPERNOVAE TO $z \approx 1.6$ AND CONSTRAINTS ON TYPE Ia PROGENITOR MODELS" (ApJ, 613, 200 [2004])

Louis-Gregory Strolger, Adam G. Riess, Tomas Dahlen, Mario Livio, Nino Panagia, Peter Challis, John L. Tonry, Alexei V. Filippenko, Ryan Chornock, Henry Ferguson, Anton Koekemoer, Bahram Mobasher, Mark Dickinson, Mauro Giavalisco, Stefano Casertano, Richard Hook, Stephane Bondin, Bruno Leibundgut, Mario Nonino, Piero Rosati, Hyron Spinrad, Charles C. Steidel, Daniel Stern, Peter M. Garnavich, Thomas Matheson, Norman Grogin, Ann Hornschemeier, Claudia Kretchmer, Victoria G. Laidler, Kyoungsoo Lee, Ray Lucas, Duilia de Mello, Leonidas A. Moustakas, Swara Ravindranath, Marin Richardson, and Edward Taylor

We have found an error in our rate calculation, modest in size, due to a computational error in the volume of shells with radius z. This error was ~20% in size; after fixing it, we get the new results described here.

We have recalculated the maximum likelihood values for each of the tested models, and the results are very encouraging. In the narrow Gaussian model, the maximum likelihood value for the mean delay time of SNe Ia has decreased, but remains large, with $\tau = 3.4$ Gyr (see Fig. E1). In the revised Table 3 we show the maximum likelihood values of τ for each tested model. We also show the range in τ that contains 95% of the most likely values for τ.

The updated version of Figure 12 given here shows the Bayesian probability distributions for each of the tested models. As can be seen, e-folding models still prefer long folding times, of at least 1 Gyr but with a preference for folding times greater than 2–3 Gyr. However, these models predict that SNe Ia are just as likely to be prompt (<1 Gyr delays) as they are to have long, 10 Gyr delay times. Such models produce poorer fits to the observed redshift distributions than the Gaussian models, primarily because they require a higher fraction of SNe Ia at very high redshifts ($z \gtrsim 1.4$) than were observed (see revised Fig. 14 given here). It is still the case that we find our narrow Gaussian model gives the best fit to the observations, now with a mean of 3.4 Gyr. This still implies that SNe Ia stem from single degenerate systems with low-mass companion stars.

Finally, there is a typographical error in the expression of the volume shown in the manuscript. The volume at redshift z is $V(z) = (4\pi/3)[D_p(z)]^3 = (4\pi/3)(1+z)^{-3}[D_L(z)]^3$, where $D_p(z)$ is the proper motion distance, and $D_L(z)$ is the luminosity distance to redshift z. The correct form of the equation has always been used in the calculations.

We thank Francisco Forster, Christian Wolfe, and Philipp Podsiadlowski of Oxford University for pointing out these errors in the manuscript.

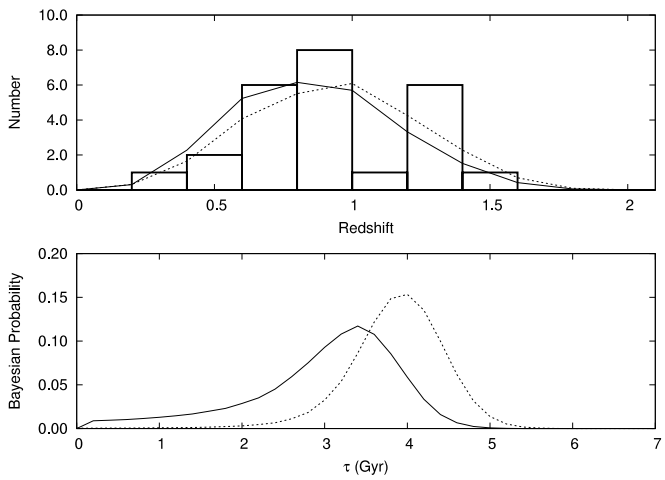

Fig. E1.—Comparison of the corrected calculations to those done in the original manuscript. *Upper panel:* The correctly predicted SN Ia redshift distribution for the narrow Gaussian delay time model (with $\tau = 4.0$ Gyr) convolved with the M1 SFR(z) is shown (*solid line*) in comparison to the erroneous calculation of the same model (*dashed line*). Also shown is the observed redshift distribution of SNe Ia, in bins of $\Delta z = 0.2$. *Lower panel:* The correctly predicted relative Bayesian probabilities for the narrow Gaussian model for all values of τ (*solid line*) compared to the previous calculation (*dashed line*).

TABLE 3

RECALCULATED LIKELIHOOD STATISTICS

Statistic	SFR Model	*e*-folding	*e*-folding w/MCO	$G(\tau, 0.5\tau)$	$G(\tau, 0.2\tau)$
Maximum likelihood τ	M1	5.4	4.4	3.0	**3.4**
	M2	2.8	2.6	2.4	2.6
95% Interval τ	M1	>1.6	>1.6	0.2–6.6	1.0–4.4
	M2	>1.0	0.8–10	0.2–4.8	0.4–3.6

NOTE.—95% intervals are for the range of most probable values of τ that encompass 95% of the total probability, within a given model. Values are given in Gyr.

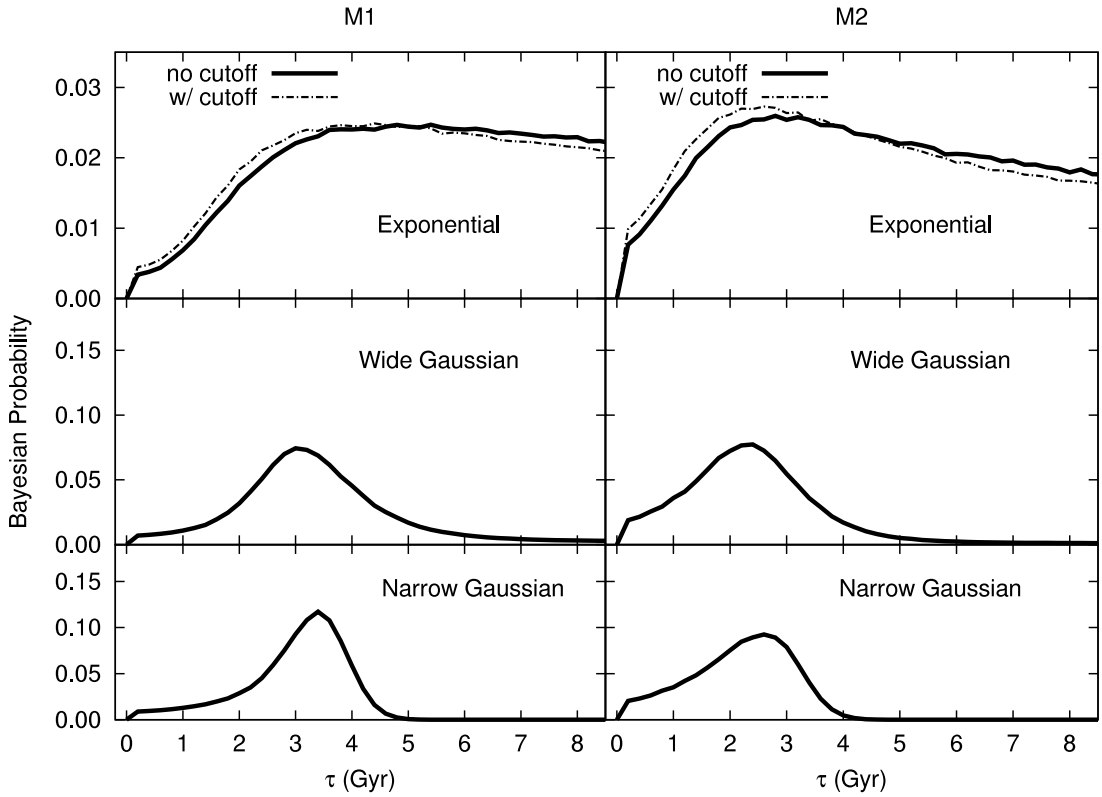

FIG. 12.—Probability distributions for the *e*-folding (*top panels, shown with and without metallicity cutoff*), wide Gaussian (*middle panels*), and narrow Gaussian (*bottom panels*) models shown as a function of τ for the M1 (*left panels*) and M2 (*right panels*) SFR histories. This figure replaces Figure 12 of the original manuscript.

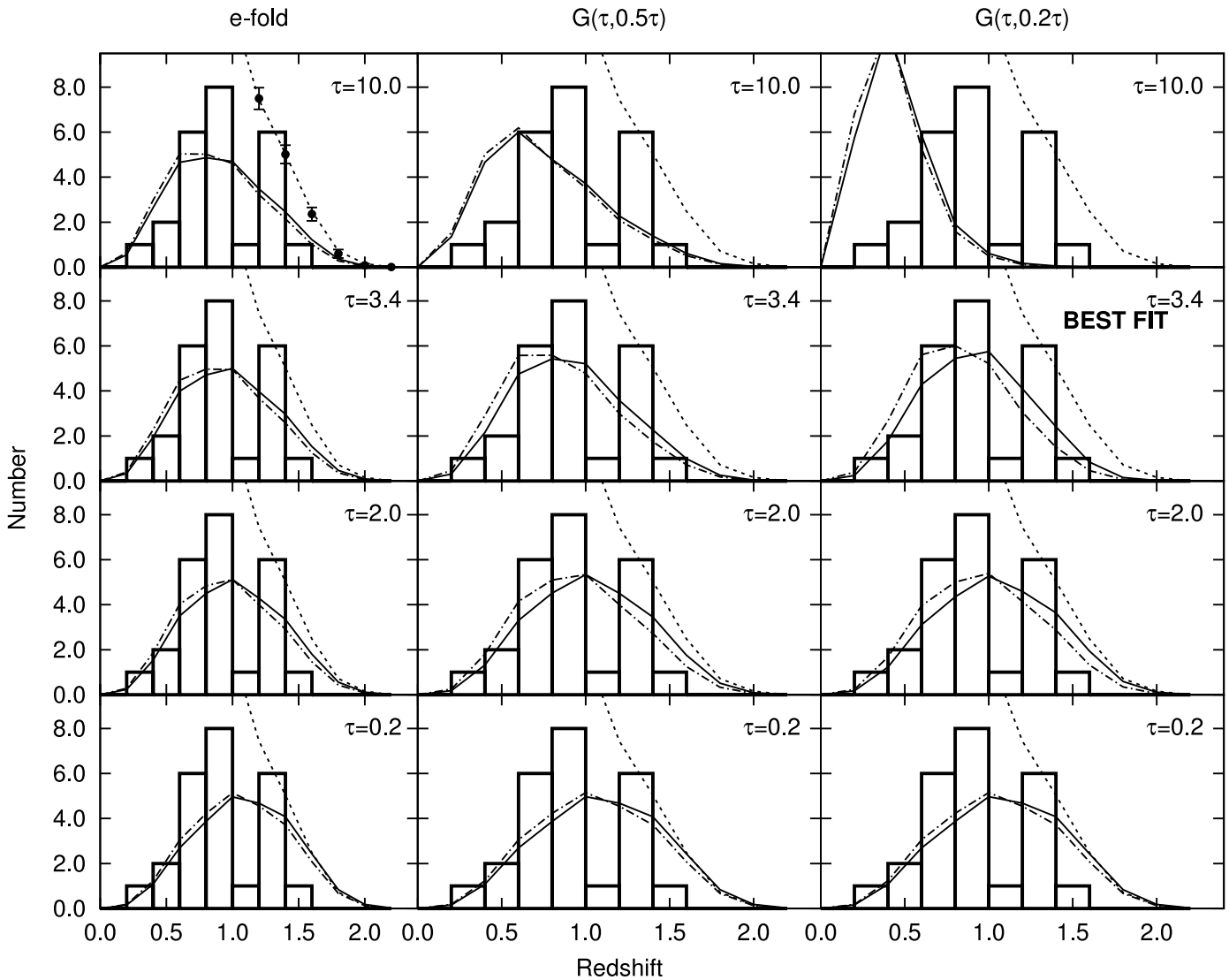

FIG. 14.—Predicted number distributions of SNe Ia for each model for selected values of τ. The solid line is for the M1 SFR(z), and the dash-dotted line is for the M2 model. The dotted line shows the control time (or survey efficiency, scaled) with redshift. The systematic effects on the control time are shown in the top left panel (*black points*). These predicted distributions are compared to the observed redshift distribution of SNe Ia, in bins of $\Delta z = 0.2$. This figure replaces Figure 14 of the original manuscript.